Applied Energy 350 (2023) 121725

Contents lists available at ScienceDirect

Applied Energy

journal homepage: www.elsevier.com/locate/apenergy

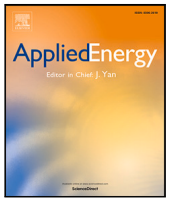

A robustness-enhanced frequency regulation scheme for power system against multiple cyber and physical emergency events

Shaohua Yang [a,b], Keng-Weng Lao [a,b,*], Hongxun Hui [a,b], Yulin Chen [c]

[a] State Key Laboratory of Internet of Things for Smart City, University of Macau, Macao, 999078, Macao Special Administrative Region of China
[b] Department of Electrical and Computer Engineering, University of Macau, Macao, 999078, Macao Special Administrative Region of China
[c] Hainan Institute of Zhejiang University, Sanya, 572000, China

ARTICLE INFO

Keywords:
Power system
Frequency regulation
Emergency events
Robust control
Lyapunov theorem

ABSTRACT

Emergency events, e.g., accidental generator outages and abrupt steeps in electric load in physical layer, and unexpected communication time delays in cyber layer, are raising increasing concerns in modern power systems, and can cause system frequency deterioration, thus threatening power energy security. However, currently there is few discussions on dealing with multiple emergency events in power system comprehensively and simultaneously. In order to counter the adverse effects caused by these various emergency events and maintain the system frequency, a robustness-enhanced frequency regulation scheme is proposed in this article based on the coordinate transformation technique and Lyapunov theorem. First, to analyze the dynamic process of the power system in contingency conditions, the model of the power system frequency regulation is reconstructed considering multiple emergency events. Furthermore, to guarantee the power system frequency stability, a virtual auxiliary surface is constructed based on the coordinate transformation technique, which can provide the control reference for frequency regulation. On this basis, a robust controller is developed to drive the system's trajectory to the proposed virtual auxiliary surface, thus guaranteeing the robustness of power system frequency, e.g., minor frequency deviation and faster recovery speed, even with emergency events. In addition, the stability of the system with the proposed controller is rigorously proved by Lyapunov theorem. Finally, the effectiveness of the proposed scheme is verified by case studies. The results show that by using the proposed scheme, the maximum frequency deviation and recovery time can be improved to about 61.11% and 46.40% of the original value under multiple emergency events, respectively. Therefore, the proposed scheme can counter well against emergency events and contribute to the power system's frequency regulation and energy security.

1. Introduction

Maintaining the system frequency at the scheduled value (e.g., 50 Hz in China and 60 Hz in the USA) is a basic requirement for the power system's safe and stable operation [1,2]. The frequency deviation may lead to severe damage and even cause the system to collapse. For example, in the UK, on Aug 9, 2019, the frequency of the Great Britain transmission system dropped from 50 Hz to 48.8 Hz, which triggered a system operators' low frequency demand disconnection for the first time in 11 years and interrupted electricity supply to approximately 1.1 million customers [3]. Similarly, in Taiwan, China, on Aug 15, 2017, the sudden shutdown of six gas generating units at the Datan power plant led to the frequency dropping, which became the worst power accident in the past 20 years in Taiwan, and affected 17 cities and about 5.92 million customers [4]. Therefore, frequency regulation is one of the most essential operating functions for the power system [5,6], which can maintain system frequency by increasing or decreasing power generation or consumption according to the frequency deviation (i.e., the deviation between the actual frequency and the scheduled frequency value) [7].

The performance of frequency regulation in the modern power system can be mainly reflected in three aspects, i.e., maximum frequency deviation, recovery time, and frequency oscillation [8]. (i) Maximum frequency deviation is the deviation between the actual system's maximum frequency value and the scheduled frequency value

* Corresponding author at: State Key Laboratory of Internet of Things for Smart City, University of Macau, Macao, 999078, Macao Special Administrative Region of China.
E-mail address: johnnylao@um.edu.mo (K.-W. Lao).

https://doi.org/10.1016/j.apenergy.2023.121725
Received 16 June 2023; Received in revised form 27 July 2023; Accepted 2 August 2023
Available online 24 August 2023

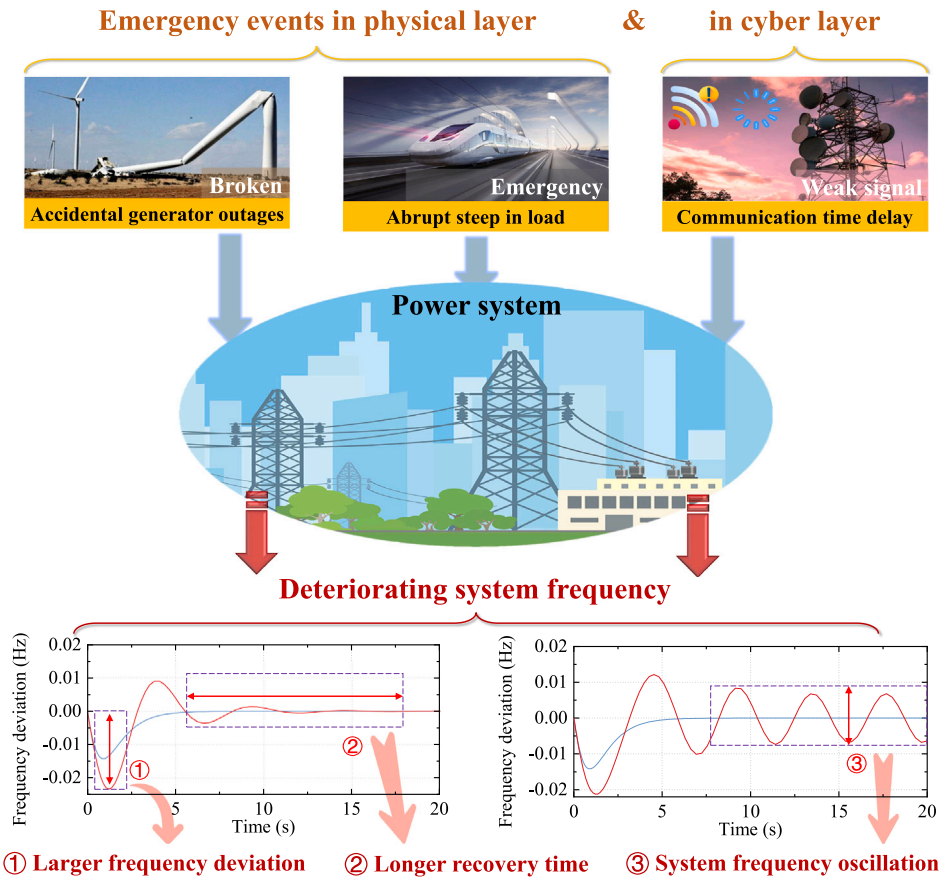

Fig. 1. Negative consequences of power systems frequency caused by cyber and physical emergency events.

(or the deviation between the scheduled frequency value and the actual system's minimum frequency value) during the whole regulation process, which is an important index to evaluate the system frequency performance [9]. In general, large maximum frequency deviation implies sharp frequency fluctuations, which ought to be avoided for the power system [10]. (ii) Recovery time denotes the time duration between the start of frequency regulation (generally when the system frequency deviation exceeds the frequency deviation threshold) and the completion of frequency regulation [11]. A fast recovery speed implies a short time for system frequency fluctuations, contributing to the frequency stability of the power system [12]. (iii) Frequency oscillation in the power system denotes the periodic or repetitive variation, typically in time, of the system frequency around the scheduled frequency, e.g., 50 Hz [13]. Frequency oscillation means that the system frequency is severely unstable, and can be quite damaging to the power system [14]. All of these performances deserve attention to better regulate the power system frequency.

Recently, several works have been developed to improve the performance of frequency regulation. For example, to achieve frequency regulation in islanded microgrids, a self-triggered distributed control is presented, which also considers the control burden of communication and computation [15]. In addition, to maintain frequency stability, a novel optimal dispatching control strategy is proposed for electric vehicle aggregators, with a high utilization efficiency of electric vehicles [16]. Moreover, a coordination control method is developed for frequency regulation in urban microgrids, which can tap flexibility from both load resources on the demand-side and distributed generators on the supply-side [17]. A two-layer coordinated control strategy is proposed for central air conditioning to offer frequency regulation services for the power system [18]. A model predictive control scheme is presented for providing frequency reserves to the electricity grid, which exploits the energy flexibility of buildings [19]. Many factors, including the burden of communication and computation, the coordination between the demand and supply sides, and the flexibility of different types of load resources, have been considered in frequency regulation, and these efforts have made significant progress.

However, one of the most crucial impact factors in the modern power system, i.e., the emergency event, has not been fully considered and addressed in the previous literature. In fact, emergency events have become a severe problem in the power system's frequency regulation [20], which can be illustrated in Fig. 1. For example, an accidental generator outage is an emergency event that can result in system frequency deviation [21]. The widespread deployment of renewable energies worldwide has made the risk of accidental generator outages higher than ever before [22], since renewable energies are heavily affected by variable environments and are more difficult for equipment maintenance due to their dispersal in remote areas [23]. Moreover, the abrupt steep (increase or decrease) in electric load requirements is another type of emergency event [24]. On the demand side of power systems, the electrification of some other industrial sectors is proceeding (e.g., transportation sector) [25]. Therefore, the situation of electric load requirement has become increasingly complex [26], which also presents potential risks [27]. For instance, the emergency braking of high-speed rail trains can cause a severe power impulse (even over 13 MW) on the power system [28], which can also cause a deviation of the system frequency [29]. Furthermore, in cyber layer, the communication time delay is also a type of critical unexpected contingencies [30]. For frequency regulation, it is necessary to measure the system frequency deviation and transfer the related signal to the control center in a timely and accurate manner [31]. However, when there is a communication time delay, the control decision is according to the frequency signal of the past time, which may cause an opposite regulation, thus leading to frequency oscillations and further deteriorating the power system frequency [32]. All of these emergency events bring new problems for

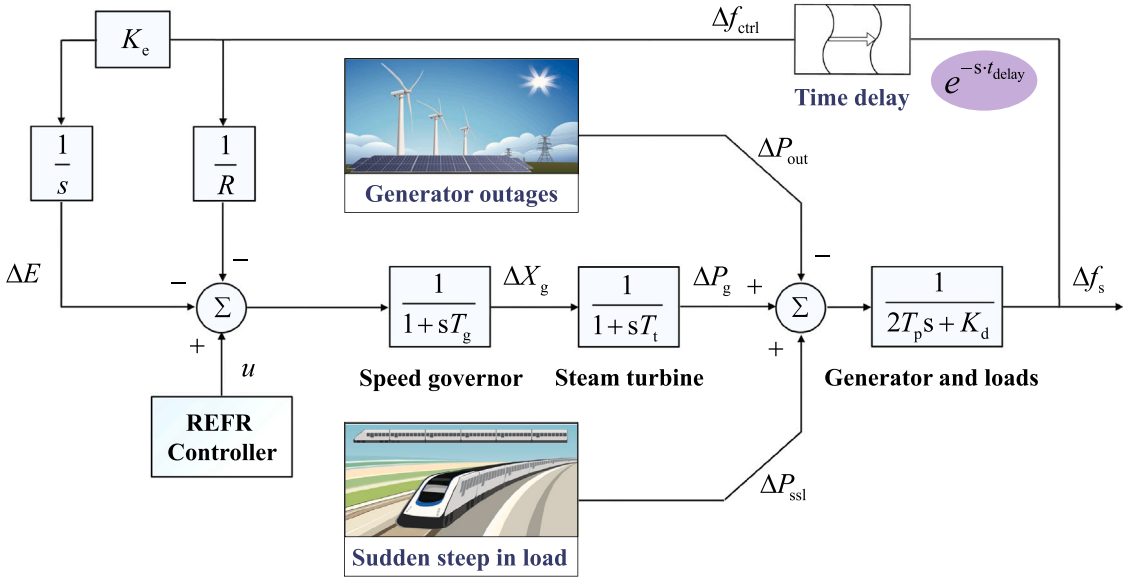

Fig. 2. The control block diagram of frequency regulation system considering emergency events.

frequency regulation, such as large frequency deviation, long recovery time, and frequency oscillation [33]. The negative consequences of these emergency events on frequency regulation can severely threaten the power energy security, which has become one of the main challenges for modern power systems [34]. How to regulate the system frequency with a tolerable deviation and fast recovery speed even during multiple cyber and physical emergency events is an essential task for power system frequency regulation.

To address this issue described above, this paper focuses on the power system frequency regulation with the problem of multiple cyber and physical emergency events. A novel robustness-enhanced frequency regulation (REFR) scheme is proposed to counter the negative consequences caused by emergencies, thus achieving high-performance frequency regulation and guaranteeing power energy security. The major contributions of this paper are threefold:

- A model of the power system frequency regulation is reconstructed considering multiple contingencies, so as to analyze the dynamic process of the power system with cyber and physical emergency events.
- A virtual auxiliary surface is constructed based on the coordinate transformation technique to ensure the system frequency stability. Based on the proposed virtual auxiliary surface, a robust controller is developed to achieve a minor frequency deviation and a faster recovery for frequency regulation, as well as to avoid frequency oscillations.
- Rigorous proofs show that the stability of power system frequency can be guaranteed by the proposed method, despite multiple emergency events, e.g., accidental generator outages, abrupt steeps in electric load requirements, and unexpected communication time delays.

The rest of this paper is organized as follows: the frequency regulation system considering multiple emergency events is modeled in Section 2. Then, a REFR scheme is proposed for the power system in Section 3. To be specific, a virtual auxiliary surface is constructed and a robust controller is developed to counter adverse impacts caused by multiple emergency events. Furthermore, the rigorous proof of stability is also given in this section. In Section 4, the effectiveness of the proposed scheme is verified by case studies. Finally, Section 5 concludes this article.

2. Model of power system frequency regulation considering multiple emergency events

As a foundation, the model of frequency regulation system with multiple emergency events is developed in this section. The control block diagram of power system frequency regulation [35] can be shown in Fig. 2. On this basis, the dynamical equations for the control block diagram can be expressed as follows:

$$\Delta\dot{f}_s(t) = -\frac{K_d}{2T_p}\Delta f(t) + \frac{1}{2T_p}\Delta P_g(t) - \frac{1}{2T_p}\Delta P_{ssl}(t) + \frac{1}{2T_p}\Delta P_{out}(t), \tag{1}$$

$$\Delta\dot{P}_g(t) = -\frac{1}{T_t}\Delta P_g(t) + \frac{1}{T_t}\Delta X_g(t), \tag{2}$$

$$\Delta\dot{X}_g(t) = -\frac{1}{RT_g}\Delta f(t) - \frac{1}{T_g}\Delta E(t) + \frac{1}{T_g}u(t) - \frac{1}{T_g}\Delta X_g(t), \tag{3}$$

$$\Delta\dot{E}(t) = K_e\Delta f(t), \tag{4}$$

where variable states $\Delta f(t)$, $\Delta P_g(t)$, $\Delta X_g(t)$, and $\Delta E(t)$ are the frequency deviation of power system, generator mechanical output deviation, governor valve position deviation, and integral control deviation, respectively; u is the control input; T_g and T_t are the time constants of speed governor and steam turbine, respectively; R, K_e, T_p and K_d are drooping characteristic, integral control gain, equivalent inertia constant and equivalent damping coefficient, respectively; $\Delta P_{out}(t)$ and $\Delta P_{ssl}(t)$ are the power disturbances caused by emergency events, i.e., accidental generator outages and abrupt steeps of load requirements, respectively, which can cause severe disruptions to the power system.

The dynamics in (1)–(4) can be formulated into a matrix form, which can be presented below:

$$\dot{\boldsymbol{x}}(t) = \boldsymbol{A}\boldsymbol{x}(t) + \boldsymbol{B}\boldsymbol{u}(t) + \boldsymbol{D}\Delta P_{out}(t) - \boldsymbol{D}\Delta P_{ssl}(t), \tag{5}$$

where $\boldsymbol{x}(t) = \begin{bmatrix}\Delta f(t) & \Delta P_g(t) & \Delta X_g(t) & \Delta E(t)\end{bmatrix}^T$ is the state vector of this state-space equation; $\boldsymbol{A}$ is the state-transition matrix; $\boldsymbol{B} = \begin{bmatrix}0 & 0 & \frac{1}{T_g} & 0\end{bmatrix}^T$ is the control matrix, which can indicate how the control signal regulates the system; $\boldsymbol{u}$ is the control input to be designed; $\boldsymbol{D} = \begin{bmatrix}-\frac{K_p}{2T_p} & 0 & 0 & 0\end{bmatrix}^T$ is the influence matrix, which can indicate how the system affected by the emergency events.

Furthermore, in cyber layer, considering the contingency arising from the communication time delay, there will be a system frequency detection error:

$$\Delta f_{err} = \Delta f_{meas} - \Delta f_{ctrl}, \tag{6}$$

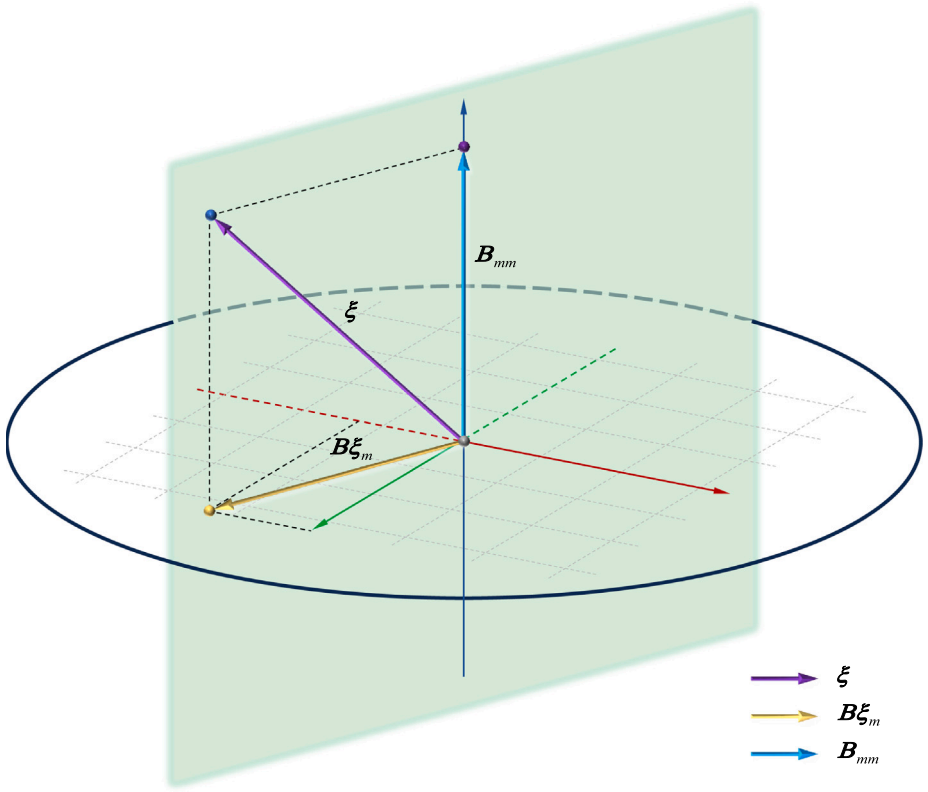

Fig. 3. The schematic diagram for the projection and decomposition of vectors.

where Δf_{err} is the detection error of system frequency for the controller; $\Delta f_{\text{meas}} = \Delta f(t_k^{\text{sd}})$ is the deviation value of system frequency measured by the PMU, which can be regarded as the exact value; t_k^{sd} is the sending time for deviation value of system frequency; $\Delta f_{\text{ctrl}} = \Delta f(t_k^{\text{rc}})$ is the deviation value of system frequency received by the controller, which is affected by the communication time delay; t_k^{rc} is the receiving time for frequency deviation value by the control center, which can be expressed as follows:

$$t_k^{\text{rc}} = t_k^{\text{sd}} - t_{\text{delay}}, \tag{7}$$

where t_{delay} denotes the delay time of communication.

Due to the system frequency detection error caused by the communication time delay, the dynamical equation of the system described in (5) has modeling errors and needs to be revised as follows:

$$\dot{\boldsymbol{x}}(t) = \boldsymbol{A}\boldsymbol{x}(t) + \boldsymbol{B}\boldsymbol{u}(t) + \boldsymbol{D}\Delta P_{\text{out}}(t) - \boldsymbol{D}\Delta P_{\text{ssl}}(t) + \boldsymbol{\epsilon}(t), \tag{8}$$

where $\boldsymbol{\epsilon}(t) = \left[\epsilon_1(t)\ \epsilon_2(t)\ \epsilon_3(t)\ \epsilon_4(t)\right]^{\text{T}}$ is the error vector describing modeling errors caused by the communication time delay, with $\epsilon_1(t) = \frac{K_{\text{d}}}{2T_{\text{p}}}\Delta f_{\text{err}}(t)$, $\epsilon_2(t) = 0$, $\epsilon_3(t) = \frac{1}{RT_{\text{g}}}\Delta f_{\text{err}}(t)$, and $\epsilon_4(t) = -K_{\text{e}}\Delta f_{\text{err}}(t)$. Since all of $\Delta P_{\text{out}}(t)$, $\Delta P_{\text{out}}(t)$, and $\boldsymbol{\epsilon}(t)$ terms are from emergency events, they can be aggregated as a contingency term. On this basis, the dynamics of power system frequency regulation can be given as follows:

$$\dot{\boldsymbol{x}}(t) = \boldsymbol{A}\boldsymbol{x}(t) + \boldsymbol{B}\boldsymbol{u}(t) + \boldsymbol{\xi}(t), \tag{9}$$

where $\boldsymbol{\xi}(t) = \boldsymbol{D}\Delta P_{\text{out}}(t) - \boldsymbol{D}\Delta P_{\text{ssl}}(t) + \boldsymbol{\epsilon}(t)$ is the contingency vector describing multiple emergency events on the power system, e.g., accidental generator outages, abrupt steeps in load requirements and unexpected communication time delays.

According to the projection of the contingency vector $\boldsymbol{\xi}$ onto the control matrix $\boldsymbol{B}$, the contingency term $\boldsymbol{\xi}$ can be decomposed into two mutually perpendicular directions. To be clear, a schematic diagram is presented in Fig. 3.

As shown in Fig. 3, the vector $\boldsymbol{\xi}$ in space is projected and decomposed into two mutually perpendicular vectors. One is the vector $\boldsymbol{B}\boldsymbol{\xi}_m$, which is related to the known control matrix $\boldsymbol{B}$, and the other is the vector $\boldsymbol{B}_{mm}$. Therefore, the definition of $\boldsymbol{B}_{mm}$ is the vector that satisfies the decomposition relation and is also mutually perpendicular to $\boldsymbol{B}\boldsymbol{\xi}_m$.

Based on the decomposition of the vector $\boldsymbol{\xi}$, and the vertical relationship between $\boldsymbol{B}\boldsymbol{\xi}_m$ and $\boldsymbol{B}_{mm}$, we have the following equation:

$$\boldsymbol{\xi} = \boldsymbol{B}\boldsymbol{\xi}_m + \boldsymbol{B}_{mm}, \tag{10}$$

$$(\boldsymbol{B}\boldsymbol{\xi}_m)^{\text{T}}\boldsymbol{B}_{mm} = \boldsymbol{0}, \tag{11}$$

where $\boldsymbol{\xi}_m$ is the projection coefficient (numeric value or vector), which can be solved as below. Two parts on the right side in (10), $\boldsymbol{B}\boldsymbol{\xi}_m$ and $\boldsymbol{B}_{mm}$, are named matched contingency and mismatched contingency in this work, respectively.

Since $(\boldsymbol{B}\boldsymbol{\xi}_m)^{\text{T}} = \boldsymbol{\xi}_m^{\text{T}}\boldsymbol{B}^{\text{T}}$ and the projection coefficient $\boldsymbol{\xi}_m$ is not zero, (11) can be rewritten as follows:

$$\boldsymbol{B}^{\text{T}}\boldsymbol{B}_{mm} = \boldsymbol{0}. \tag{12}$$

The projection coefficient $\boldsymbol{\xi}_m$ can be uniquely determined by left-multiplying $\boldsymbol{B}^{\text{T}}$ for (10), as follows:

$$\boldsymbol{B}^{\text{T}}\boldsymbol{\xi} = \boldsymbol{B}^{\text{T}}\boldsymbol{B}\boldsymbol{\xi}_m + \boldsymbol{B}^{\text{T}}\boldsymbol{B}_{mm}. \tag{13}$$

Considering the relationship in (12) and rearranging (13), the projection coefficient $\boldsymbol{\xi}_m$ can be obtained as follows:

$$\boldsymbol{\xi}_m = \frac{\boldsymbol{B}^{\text{T}}\boldsymbol{\xi} - \boldsymbol{B}^{\text{T}}\boldsymbol{B}_{mm}}{\|\boldsymbol{B}\|^2} = \frac{\boldsymbol{B}^{\text{T}}\boldsymbol{\xi}}{\|\boldsymbol{B}\|^2}, \tag{14}$$

where $\|\cdot\|$ stands for the 2-norm. Then, both the matched contingency $\boldsymbol{B}\boldsymbol{\xi}_m$ and the mismatched contingency $\boldsymbol{B}_{mm}$ can be uniquely determined by projecting and decomposing original contingency term $\boldsymbol{\xi}$ as follows:

$$\begin{cases} \boldsymbol{B}\boldsymbol{\xi}_m = \boldsymbol{B}\frac{\boldsymbol{B}^{\text{T}}\boldsymbol{\xi}}{\|\boldsymbol{B}\|^2}, \\ \boldsymbol{B}_{mm} = \boldsymbol{\xi} - \boldsymbol{B}\frac{\boldsymbol{B}^{\text{T}}\boldsymbol{\xi}}{\|\boldsymbol{B}\|^2}. \end{cases} \tag{15}$$

Moreover, two assumptions are held for the system as follows.

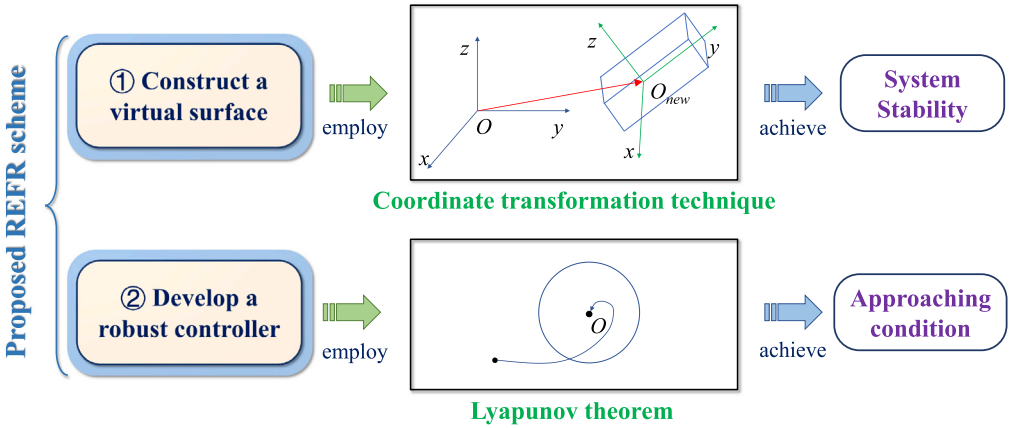

Fig. 4. The overall framework of the proposed REFR scheme.

Assumption 1. The pair $(\boldsymbol{A}, \boldsymbol{B})$ is controllable.

Assumption 2. The contingency term ξ is not infinite but bounded, and the mismatched contingency has a limited impact on the power system.

These assumptions are reasonable since the frequency regulation system is controllable, and the impact on the power system caused by emergency events is generally within a certain range. In detail, upper boundaries exist for the contingency terms, which can be shown as follows:

$$\|\xi_m\| < \beta_m, \ \|\boldsymbol{B}_{mm}\| < \beta_{mm}, \tag{16}$$

where β_m and β_{mm} are the upper boundaries for the matched and the mismatched contingency, respectively.

On this basis, the dynamics of the system considering multiple emergency events can be formulated as follows:

$$\dot{\boldsymbol{x}}(t) = \boldsymbol{A}\boldsymbol{x}(t) + \boldsymbol{B}\boldsymbol{u}(t) + \boldsymbol{B}\xi_m(t) + \boldsymbol{B}_{mm}(t). \tag{17}$$

In this section, the model of frequency regulation system is developed with multiple cyber and physical emergency events under investigation, which can be utilized to analyze the dynamic process of the power system considering emergency events.

3. Proposed robustness-enhanced frequency regulation scheme

In order to counter the negative consequences of emergency events and achieve high-performance frequency regulation, a robustness-enhanced frequency regulation (REFR) scheme is proposed in this section.

3.1. Overall framework of the proposed REFR scheme

The overall framework of the proposed REFR scheme is illustrated in Fig. 4. In particular, there exists a main challenge in designing the REFR scheme. That is how to guarantee the system frequency stability under multiple emergency events, e.g., unexpected communication time delays. To address this issue, firstly a virtual auxiliary surface is constructed based on the coordinate transformation technique to provide a surface for control reference.

Definition. The approaching condition denotes that the system's trajectory can approach the constructed virtual auxiliary surface.

The constructed surface can act as a target that the system's trajectory needs to be driven to, until the approaching condition is satisfied. In this way, the stability of the system can then be guaranteed by the eigenvalue assignment method, even under unexpected disturbances caused by emergency events. Furthermore, it is because the approaching condition is so vital that a robust controller has to be developed, so as to ensure the approaching condition and make the system's trajectory stay on the virtual auxiliary surface afterward. With the proposed robust controller based on Lyapunov theorem, the approaching condition can be satisfied, and high-performance control for power system frequency can be achieved even under multiple emergency events.

Both the surface construction and controller development of the proposed scheme are described in the following subsections.

3.2. Virtual auxiliary surface construction based on coordinate transformation technique

In order to enhance the robustness of emergency events, a virtual auxiliary surface is constructed based on the coordinate transformation technique. This constructed surface can provide the reference for the control of frequency regulation, thus guaranteeing the system frequency stability, which is shown below:

$$\boldsymbol{\Gamma}\boldsymbol{x}(t) = 0, \tag{18}$$

where $\boldsymbol{\Gamma}$ is the auxiliary surface matrix and should be constructed to guarantee that matrix $\boldsymbol{\Gamma}\boldsymbol{B}$ is non-singular. In this work, the matrix $\boldsymbol{\Gamma}$ is constructed to satisfy the equation as follows:

$$\boldsymbol{\Gamma} = \begin{bmatrix} \boldsymbol{K} & \boldsymbol{I} \end{bmatrix} \boldsymbol{T}, \tag{19}$$

where $\boldsymbol{K}$ is the state feedback control matrix, which can be designed according to the desired eigenvalues; $\boldsymbol{I}$ is the identity matrix; $\boldsymbol{T}$ is the coordinate transformation matrix which satisfies the following equation:

$$\boldsymbol{T} = \begin{bmatrix} \boldsymbol{B}_r^{\mathrm{T}} \\ (\boldsymbol{B}^{\mathrm{T}}\boldsymbol{B})^{-1}\boldsymbol{B}^{\mathrm{T}} \end{bmatrix}, \tag{20}$$

where $\boldsymbol{B}_r$ is a matrix satisfying the following relationship $\boldsymbol{B}_{mm} = \boldsymbol{B}_r\xi_{mm}$; and ξ_{mm} is a coefficient (numeric value or vector). On this basis, considering (12), we have:

$$\boldsymbol{B}^{\mathrm{T}}\boldsymbol{B}_r = \boldsymbol{0}. \tag{21}$$

Then, according to the equation of virtual auxiliary surface in (18), the surface function can be given as follows:

$$\boldsymbol{s}(t) = \boldsymbol{\Gamma}\boldsymbol{x}(t). \tag{22}$$

The surface function described in (22) is a function of $\boldsymbol{x}(t)$. Therefore, it varies with the system's state variables. When the approaching condition is satisfied, it means the trajectory of the system achieves and maintains on the constructed virtual auxiliary surface, and in this case, the surface function meets the following relationship:

$$\boldsymbol{s}(t) = \boldsymbol{0}. \tag{23}$$

With the constructed virtual auxiliary surface, the main result of the frequency regulation system considering multiple emergency events can be given, which is presented below.

Theorem 1. *When the approaching condition is satisfied for the constructed virtual auxiliary surface, i.e., $s(t) = \mathbf{0}$, the dynamic performance of the frequency regulation system is stable.*

Proof. According to the coordinate transformation matrix $\boldsymbol{T}$ in (20), the new coordinates $\boldsymbol{z}(t)$ can be obtained as follows:

$$\boldsymbol{z}(t) = \boldsymbol{T}\boldsymbol{x}(t) = \begin{bmatrix} \boldsymbol{y}(t) \\ \boldsymbol{v}(t) \end{bmatrix}, \tag{24}$$

where $\boldsymbol{y}(t) \in \mathbb{R}^{n-m}$ and $\boldsymbol{v}(t) \in \mathbb{R}^{m}$ are two parts of the new coordinates. Moreover, the control matrix can be transformed and partitioned as a zero matrix and an identity matrix, shown as follows:

$$\boldsymbol{T}\boldsymbol{B} = \begin{bmatrix} \boldsymbol{B}_r^{\mathrm{T}} \\ (\boldsymbol{B}^{\mathrm{T}}\boldsymbol{B})^{-1}\boldsymbol{B}^{\mathrm{T}} \end{bmatrix} \boldsymbol{B} = \begin{bmatrix} \boldsymbol{0} \\ \boldsymbol{I} \end{bmatrix}. \tag{25}$$

Based on the coordinate transformation operation, the frequency regulation system in (17) can be rewritten as follows:

$$\begin{aligned} \dot{\boldsymbol{z}}(t) &= \boldsymbol{T}\dot{\boldsymbol{x}}(t) \\ &= \boldsymbol{T}\boldsymbol{A}\boldsymbol{x}(t) + \boldsymbol{T}\boldsymbol{B}\boldsymbol{u}(t) + \boldsymbol{T}\boldsymbol{B}\boldsymbol{\xi}_m(t) + \boldsymbol{T}\boldsymbol{B}_{mm}(t) \\ &= \boldsymbol{T}\boldsymbol{A}\boldsymbol{T}^{-1}\boldsymbol{z}(t) + \begin{bmatrix} \boldsymbol{0} \\ \boldsymbol{I} \end{bmatrix}\boldsymbol{u}(t) + \begin{bmatrix} \boldsymbol{0} \\ \boldsymbol{I} \end{bmatrix}\boldsymbol{\xi}_m(t) + \boldsymbol{T}\boldsymbol{B}_{mm}(t), \end{aligned} \tag{26}$$

where

$$\boldsymbol{T}\boldsymbol{A}\boldsymbol{T}^{-1} = \begin{bmatrix} \boldsymbol{H}_{11} & \boldsymbol{H}_{12} \\ \boldsymbol{H}_{21} & \boldsymbol{H}_{22} \end{bmatrix}.$$

Combining (20), (24), and (26), the power system considered emergency events can be shown as follows:

$$\dot{\boldsymbol{y}}(t) = \boldsymbol{H}_{11}\boldsymbol{y}(t) + \boldsymbol{H}_{12}\boldsymbol{v}(t) + \|\boldsymbol{B}_r\|\boldsymbol{\xi}_{mm}(t), \tag{27}$$

$$\dot{\boldsymbol{v}}(t) = \boldsymbol{H}_{21}\boldsymbol{y}(t) + \boldsymbol{H}_{22}\boldsymbol{v}(t) + \boldsymbol{I}\boldsymbol{u}(t) + \boldsymbol{I}\boldsymbol{\xi}_m(t). \tag{28}$$

The auxiliary surface matrix in the new coordinate system can be partitioned as follows:

$$\boldsymbol{\Gamma}\boldsymbol{T}^{-1} = \begin{bmatrix} \boldsymbol{K} & \boldsymbol{I} \end{bmatrix}\boldsymbol{T}\boldsymbol{T}^{-1} = \begin{bmatrix} \boldsymbol{K} & \boldsymbol{I} \end{bmatrix}. \tag{29}$$

Since the approaching condition is satisfied, i.e., $s(t) = \mathbf{0}$, we have:

$$\boldsymbol{s}(t) = \boldsymbol{\Gamma}\boldsymbol{T}^{-1}\boldsymbol{z}(t) = \begin{bmatrix} \boldsymbol{K} & \boldsymbol{I} \end{bmatrix}\begin{bmatrix} \boldsymbol{y}(t) \\ \boldsymbol{v}(t) \end{bmatrix} = \boldsymbol{0}. \tag{30}$$

Moreover, since identity matrix $\boldsymbol{I}$ is non-singular, the relationship in (30) can be rewritten as follows:

$$\boldsymbol{v}(t) = -\boldsymbol{K}\boldsymbol{y}(t). \tag{31}$$

Based on the state feedback control theorem, the matrix $\boldsymbol{K}$ can be determined by the eigenvalue assignment method to satisfy the inequality as follows:

$$\mathrm{Re}(\lambda_i(\boldsymbol{H}_{11} - \boldsymbol{H}_{12}\boldsymbol{K})) < 0, \ \text{for } i = 1, 2, \ \dots, n-m, \tag{32}$$

where $\lambda(\cdot)$ stands for the eigenvalue; $\mathrm{Re}(\cdot)$ represents the real part of eigenvalues. On this basis, the system in (27) can be considered isolation with $\boldsymbol{y}(t)$ thought of as the state vector and $\boldsymbol{v}(t)$ as a virtual control input, then the system can be thought of as a closed-loop system applying the feedback controller in (31), which can be reformulated as follows:

$$\begin{aligned} \dot{\boldsymbol{y}}(t) &= \boldsymbol{H}_{11}\boldsymbol{y}(t) - \boldsymbol{H}_{12}\boldsymbol{K}\boldsymbol{y}(t) + \|\boldsymbol{B}_r\|\boldsymbol{\xi}_{mm}(t) \\ &= \underbrace{(\boldsymbol{H}_{11} - \boldsymbol{H}_{12}\boldsymbol{K})}_{\boldsymbol{A}_s}\boldsymbol{y}(t) + \|\boldsymbol{B}_r\|\boldsymbol{\xi}_{mm}(t). \end{aligned} \tag{33}$$

The stability of the system is determined by the first term, specifically by the state transfer matrix $\boldsymbol{A}_s$, as the second term in (33) is uncoupled from the state variable $\boldsymbol{y}(t)$. Furthermore, since all the eigenvalues of $\boldsymbol{A}_s$ have a negative real part as shown in (32), the system in (33) and the variable state $\boldsymbol{y}(t)$ can be stable. Moreover, according to the linear relationship shown in (31), variable state $\boldsymbol{v}(t)$ can also be stable with state vector $\boldsymbol{y}(t)$. Performing an inverse transformation on the $\boldsymbol{z}(t) = [\boldsymbol{y}(t)\ \boldsymbol{v}(t)]^{\mathrm{T}}$ by using the coordinate transformation matrix $\boldsymbol{T}$, it is easy to know that all the state variable $\boldsymbol{x}(t)$ in the original coordinate system is stable with $\boldsymbol{z}(t)$, i.e., the dynamics of frequency regulation system in (17) can be stable. The proof is complete. ■

Theorem 1 shows that the virtual auxiliary surface is constructed successfully. This is because through the constructed surface in (18), the stability of frequency regulation system can be guaranteed, even with multiple emergency events.

3.3. Robust controller design

A virtual auxiliary surface is constructed in the preceding section to ensure stability when the approaching condition is satisfied. However, the problem of how to make the system's trajectory approach the virtual auxiliary surface still need to be solved. To address this problem, a robust controller of the proposed REFR scheme is designed to drive the trajectory to and maintain on the designed surface. The controller of the proposed REFR scheme can be shown as follows:

$$\boldsymbol{u}(t) = -(\boldsymbol{\Gamma}\boldsymbol{B})^{-1}\boldsymbol{\Gamma}\boldsymbol{A}\boldsymbol{x}(t) - (\delta + \sigma)\frac{\boldsymbol{s}(t)}{\|\boldsymbol{s}(t)\|}, \tag{34}$$

where σ is a positive constant; δ is a parameter satisfying the following equation:

$$\delta = \beta_m + \|((\boldsymbol{\Gamma}\boldsymbol{B})^{-1}\boldsymbol{\Gamma})\|\beta_{mm}. \tag{35}$$

On this basis, the main result of the approaching condition can be given, which is presented below.

Theorem 2. *With the controller designed in (34), the system's trajectory can be guaranteed to approach the constructed auxiliary surface in (18), i.e., the approaching condition is satisfied.*

Proof. A Lyapunov function is considered as follows:

$$V(t) = \boldsymbol{s}^{\mathrm{T}}(t)\boldsymbol{s}(t). \tag{36}$$

When $\boldsymbol{s}(t) = 0$, i.e., the surface function is equal to zero, then the approaching condition is satisfied as shown in (23).

When $\boldsymbol{s}(t) \neq 0$, then the Lyapunov function $V(t)$ is always greater than zero. Moreover, combining (17), (22), and (36) yields the derivative of the Lyapunov function:

$$\begin{aligned} \dot{V}(t) &= \boldsymbol{s}^{\mathrm{T}}(t)\dot{\boldsymbol{s}}(t) + \dot{\boldsymbol{s}}^{\mathrm{T}}(t)\boldsymbol{s}(t) \\ &= 2\boldsymbol{s}^{\mathrm{T}}(t)\dot{\boldsymbol{s}}(t) = 2\boldsymbol{s}^{\mathrm{T}}(t)\boldsymbol{\Gamma}\dot{\boldsymbol{x}}(t) \\ &= 2\boldsymbol{s}^{\mathrm{T}}(t)\boldsymbol{\Gamma}[\boldsymbol{A}\boldsymbol{x}(t) + \boldsymbol{B}\boldsymbol{u}(t) + \boldsymbol{B}\boldsymbol{\xi}_m(t) + \boldsymbol{B}_{mm}(t)]. \end{aligned} \tag{37}$$

According to the proposed controller in (34) and (35), and substituting (34) into (37) further yields the derivative as follows:

$$\begin{aligned} \dot{V}(t) &= 2\boldsymbol{s}^{\mathrm{T}}(t)\boldsymbol{\Gamma}[\boldsymbol{A}\boldsymbol{x}(t) + \boldsymbol{B}[-\boldsymbol{B}^{-1}\boldsymbol{\Gamma}^{-1}\boldsymbol{\Gamma}\boldsymbol{A}\boldsymbol{x}(t) - (\delta + \sigma)\frac{\boldsymbol{s}(t)}{\|\boldsymbol{s}(t)\|}] \\ &\quad + \boldsymbol{B}\boldsymbol{\xi}_m(t) + \boldsymbol{B}_{mm}(t)] \\ &= 2\boldsymbol{s}^{\mathrm{T}}(t)\boldsymbol{\Gamma}[\boldsymbol{A}\boldsymbol{x}(t) - \boldsymbol{A}\boldsymbol{x}(t) + \boldsymbol{B}[-(\delta + \sigma)\frac{\boldsymbol{s}(t)}{\|\boldsymbol{s}(t)\|}] + \boldsymbol{B}\boldsymbol{\xi}_m(t) + \boldsymbol{B}_{mm}(t)] \\ &= 2\boldsymbol{s}^{\mathrm{T}}(t)[-\boldsymbol{\Gamma}\boldsymbol{B}(\delta + \sigma)\frac{\boldsymbol{s}(t)}{\|\boldsymbol{s}(t)\|} + \boldsymbol{\Gamma}\boldsymbol{B}\boldsymbol{\xi}_m(t) + \boldsymbol{\Gamma}\boldsymbol{B}_{mm}(t)]. \end{aligned} \tag{38}$$

Then, considering $\boldsymbol{\Gamma}\boldsymbol{B}$ is an identity matrix and substituting (35) into (38) further yields the following derivative:

$$\begin{aligned} \dot{V}(t) =& 2\boldsymbol{s}^{\mathrm{T}}(t)[-\boldsymbol{\Gamma}\boldsymbol{B}([\beta_m + \|((\boldsymbol{\Gamma}\boldsymbol{B})^{-1}\boldsymbol{\Gamma})\|\beta_{mm}] + \sigma)\frac{\boldsymbol{s}(t)}{\|\boldsymbol{s}(t)\|} + \boldsymbol{\Gamma}\boldsymbol{B}\boldsymbol{\xi}_m(t) \\ &+ \boldsymbol{\Gamma}\boldsymbol{B}_{mm}(t)] \end{aligned}$$

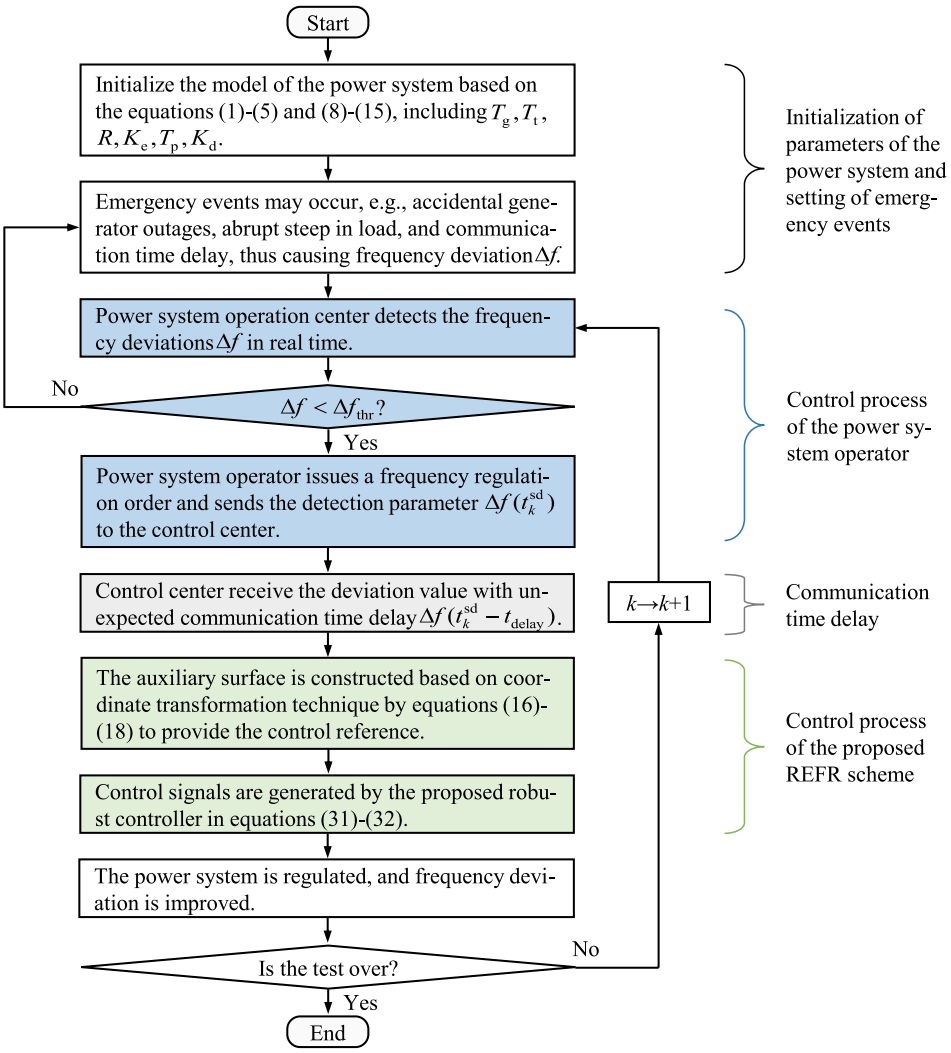

Fig. 5. The implementation procedure of the proposed REFR scheme to overcome multiple emergency events.

$$=-2\boldsymbol{s}^{\mathrm{T}}(t)(\beta_m + \|((\boldsymbol{\Gamma B})^{-1}\boldsymbol{\Gamma}\|\beta_{mm})\frac{\boldsymbol{s}(t)}{\|\boldsymbol{s}(t)\|}$$
$$-2\sigma\|\boldsymbol{s}(t)\| + 2\boldsymbol{s}^{\mathrm{T}}(t)\left[\boldsymbol{\xi}_m(t) + (\boldsymbol{\Gamma B})^{-1}\boldsymbol{\Gamma}\boldsymbol{B}_{mm}(t)\right]. \quad (39)$$

Combining (16) and (39) yields the following inequation:

$$\begin{aligned}\dot{V}(t) &< -2\|\boldsymbol{s}(t)\| \cdot \|\boldsymbol{\xi}_m(t)\| - 2\|\boldsymbol{s}(t)\| \cdot \|((\boldsymbol{\Gamma B})^{-1}\boldsymbol{\Gamma}\| \cdot \|\boldsymbol{B}_{mm}(t)\| \\ &\quad - 2\sigma\|\boldsymbol{s}(t)\| + 2\boldsymbol{s}^{\mathrm{T}}(t)\boldsymbol{\xi}_m(t) + 2\boldsymbol{s}^{\mathrm{T}}(t)(\boldsymbol{\Gamma B})^{-1}\boldsymbol{\Gamma}\boldsymbol{B}_{mm}(t) \\ &\leq -2\|\boldsymbol{s}(t)\| \cdot \|\boldsymbol{\xi}_m(t)\| - 2\sigma\|\boldsymbol{s}(t)\| + 2\boldsymbol{s}^{\mathrm{T}}(t)\boldsymbol{\xi}_m(t) \\ &\leq -2\sigma\|\boldsymbol{s}(t)\| < 0. \end{aligned} \quad (40)$$

According to Eqs. (36) and (40), it is found that when $\boldsymbol{s}(t) \neq 0$, the Lyapunov function $V(t) > 0$ and its derivative $\dot{V}(t) < 0$. Based on Lyapunov theorem, the Lyapunov function $V(t)$ can always converge to zero. Furthermore, the surface function $\boldsymbol{s}(t)$ can also converge to zero since it is contained in the Lyapunov function. This implies the system's trajectory can always approach the virtual auxiliary surface and stay there afterward, i.e., the approaching condition can be satisfied. The proof is complete. ■

Theorem 2 shows that with the proposed robust controller in (34), the approaching condition can be satisfied, despite multiple emergency events. This implies the controller is designed successfully. Moreover, Theorem 1 indicates that when the approaching condition is satisfied for the constructed virtual auxiliary surface, the stability of system frequency can be guaranteed. This means by using the proposed REFR scheme based on the constructed surface and the designed controller, the stability of power system frequency can be guaranteed, even with multiple emergency events.

4. Case studies

4.1. Test system

In this section, the power system in Fig. 2 is adopted as the test system to validate the effectiveness of the proposed REFR scheme against multiple cyber and physical emergency events. The generation capacity and the scheduled frequency of the power system are 800 MW and 50 Hz, respectively [32]. The time constants of the speed governor (T_g) and the steam turbine (T_t) are 0.1 s and 0.3 s, respectively [36]. The drooping characteristic (R) and the integral control gain (K_e) are 0.05 and 21, respectively [36]. The equivalent inertia constant (T_p) and the equivalent damping coefficient (K_d) are 10 and 1, respectively [32].

The test system is formulated by the Simulink of Matlab R2021a. The implementation procedure of the test system is shown in Fig. 5. After the initialization and setting, the power system operation center monitors the system frequency in real time. When emergency events occur, such as accidental generator outages, abrupt steeps in electric load, and unexpected communication time delays, the system frequency will deviate from the scheduled frequency. In practical applications, if frequency deviation Δf exceeds the frequency deviation threshold,

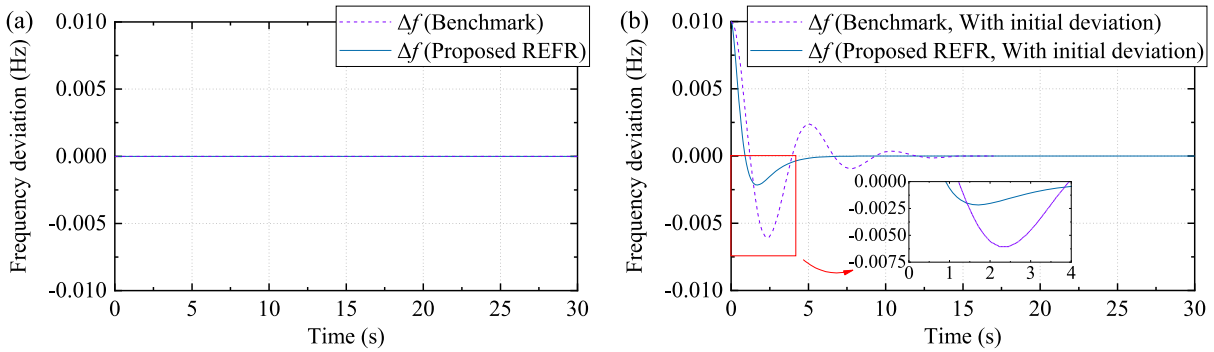

Fig. 6. Normal operation cases for frequency regulation performance without emergency event (a) also without initial deviation of frequency; (b) with 0.01 Hz initial deviation of frequency.

e.g., f_{thr} = 0.001 Hz, the system operator will issue a frequency regulation order with the detected parameter about frequency deviation. After receiving the order, the frequency regulation is started through the proposed REFR scheme according to the received detection parameter, which may be inaccurate due to communication time delay. An auxiliary surface is constructed based on the coordinate transformation technique by Eqs. (15)–(17) to provide a control reference. On this basis, the control signal is generated by the controller described in Eqs. (30)–(31). As a result, the frequency deviation of power system will be improved. The total test time is set to 30 s (or other value). If the test is not over, the operation center continuously detects the system frequency, and the frequency regulation will continuously. The system frequency is monitored by smart meters, and the frequency regulation will continue until the frequency deviation Δf is constantly less than the threshold, then this round of frequency regulation can be regarded as complete. Finally, if a new emergency event occurs and causes sufficient frequency deviation, the process will enter the next round of frequency regulation.

The proposed REFR scheme is validated in one normal case and four emergency cases, for a total of five cases. Symbols C-0, C-1, C-2, C-3, C-4, and C-5 represent the normal operation case and emergency case 1, emergency case 2, emergency case 3, emergency case 4, and emergency case 5, respectively, which are specifically listed as follows.

[C-0]: Normal operation case without any emergency event;

[C-1]: Frequency regulation performance with accidental generator outages (emergency event in physical layer);

[C-2]: Frequency regulation performance with abrupt steeps in electric load (emergency event in physical layer);

[C-3]: Frequency regulation performance with communication time delay (emergency event in cyber layer);

[C-4]: Frequency regulation performance with multiple cyber and physical emergency events simultaneously;

[C-5]: Frequency regulation performance with emergency events over a long period of time.

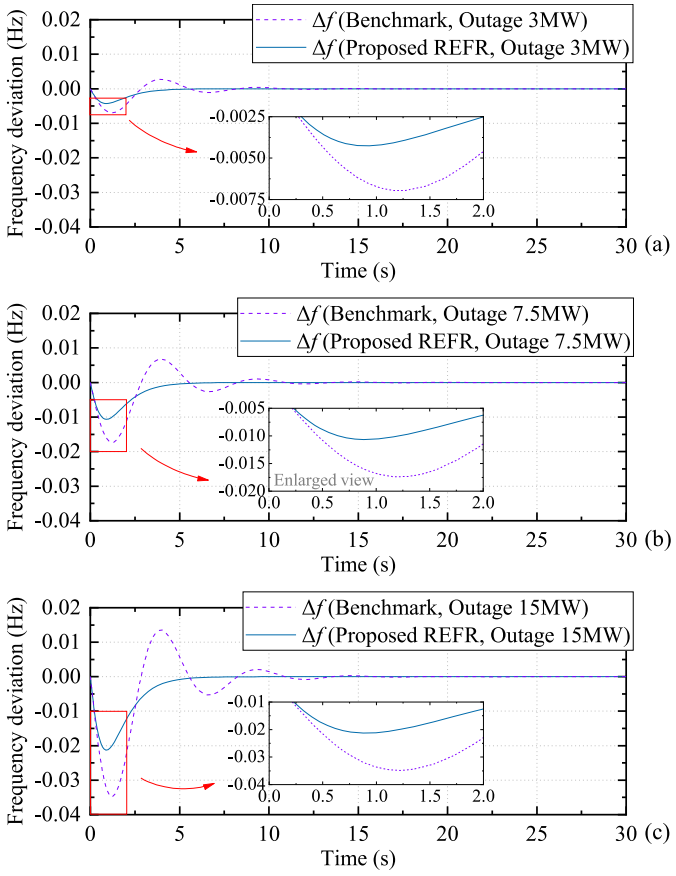

Fig. 7. Frequency regulation performance with accidental generator outages (a) 3 MW; (b) 7.5 MW; (c) 15 MW.

4.2. Normal operation case without any emergency event

The REFR method is proposed to counter the adverse impacts caused by emergency events. However, it is critical that it can be applied to normal operating situations without any emergency event. Therefore, in this subsection, the effectiveness of the proposed REFR method is verified in two normal operation cases, i.e., (a) without emergency event and initial deviation (b) without emergency event but with 0.01 Hz initial deviation of frequency. Based on the proposed method, the frequency regulation performance with these two normal operation cases can be shown in Fig. 6(a) and (b), respectively.

From Fig. 6(a), it is shown that the frequency deviation is always zero with and without the proposed REFR method. It is reasonable since the initial deviation of frequency is already zero. This indicates that the proposed REFR method will no longer change the control results if the control target has been achieved, and this verifies the effectiveness of the proposed method in the regular situation.

The recovery time and the maximum frequency deviation are essential indicators of the frequency regulation process. The recovery time can be expressed as follows:

$$\Delta T = t_{\text{end}} - t_{\text{start}}, \tag{41}$$

where t_{end} indicates the time when frequency regulation ends, and t_{start} denotes the time when frequency regulation starts. In addition, the maximum frequency deviation can be expressed by the following equation:

$$f_{\max} = max\{(max\{f(t)\} - f_s), (min\{f(t)\} - f_s)\}, \ \forall t \in \mathcal{T}, \tag{42}$$

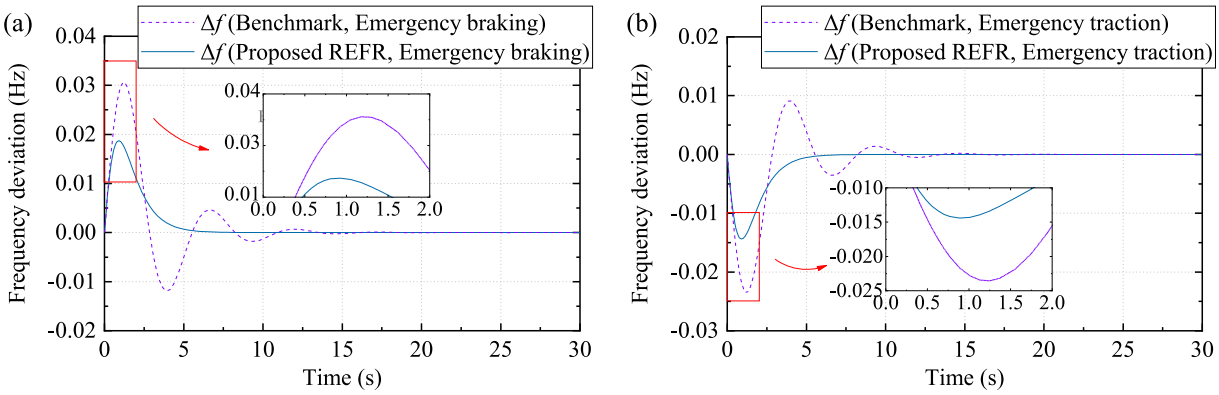

Fig. 8. Frequency regulation performance with abrupt steeps in electric load (a) emergency braking of the high-speed rail train; (b) emergency traction of the high-speed rail train.

where $f_{\max}$ is the maximum frequency deviation; $max\{\cdot\}$ denotes the function that gets the maximum value; $f(t)$ is the system frequency at time t; $min\{\cdot\}$ denotes the function that gets the minimum value; f_s is the scheduled frequency; and $\mathcal{T}$ is the time set of the frequency regulation process.

On this basis, from Fig. 6(b), it is shown that the recovery time and the maximum frequency deviation of the original are about 6.35 s and 0.0061 Hz, respectively. Moreover, the recovery time and the maximum frequency deviation with the proposed method are only about 3.11s and 0.0022 Hz, respectively. The recovery time of the proposed method is significantly shorter than the original one, about 48.98%. In addition, the maximum frequency deviation of the proposed method is only 36.07% of the original value. This implies that by using the proposed method, the power system's frequency fluctuations can be minor, and the recovery can be faster. Therefore, our proposed REFR method is high-performance and can facilitate frequency stability of power systems under normal operating situations without any emergency event.

4.3. Frequency regulation performance with accidental generator outages

In this case, some emergency events (i.e., accidental generator outages) occur on the physical layer of the power system. Taking the double-fed induction generator (DFIG) of wind farm as an example, it is assumed that there are 2, 5, and 10 DFIGs accidentally out of power in three different scenarios, respectively. According to the actual wind farm in northwest China, the generation capacity of the DFIG is 1.5 MW [37]. This means in the three scenarios, the power shocks to the power system due to accidental generator outages can be 3 MW, 7.5 MW, and 15 MW, respectively. Based on the proposed method, the frequency regulation performance with different levels of accidental generator outages is illustrated in Fig. 7.

From Fig. 7, the proposed method can well counter the adverse impact arising from accidental generator outages. Moreover, it can be known that regardless of the power shocks from the generator outages (3 MW, 7.5 MW, or 15 MW), the system frequency with the proposed method have a shorter recovery time and a minor maximum frequency deviation.

Taking the outage of 5 DFIGs as an example, as shown in Fig. 7(b), the original maximum frequency deviation deteriorates to about 0.0174 Hz due to the outage of generators. However, by using the proposed method, the maximum frequency deviation is only about 0.0106 Hz, which is only 60.92% of the original value. In addition, the original recovery time deteriorates to about 9.81 s because of generator outages. However, by using the proposed method, the recovery time is only about 4.19 s, which is also obviously shorter and only 42.71% of the original recovery time. Therefore, the proposed method can contribute to the power system frequency regulation with accidental generator outages.

4.4. Frequency regulation performance with abrupt steeps in electric load

In this part, some abrupt steeps in electric load occur in the power system. This is practical since, for instance, emergency braking and emergency traction of high-speed rail train, as well as attacks on demand-side flexible resources, can lead to abrupt steeps in electric load [38]. For this case study, emergency events of high-speed rail train are taken as examples for the test. According to the actual parameters of the 350 km/h standard electric multiple unit (EMU) train in China Railway Rolling Stock (CRRC) Corporation Limited, the traction power and braking power of the entire EMU is 10.140MW and 13.182 MW, respectively [28]. The frequency regulation performance with emergency braking and emergency traction of the high-speed rail train is shown in Fig. 8.

From Fig. 8, it can be seen that no matter with emergency braking or emergency traction, the recovery time can always be shorter, and the maximum frequency deviation can always be minor by using the proposed method.

To be specific, under the emergency braking scenario, the maximum frequency deviation with the proposed method is reduced from the original about 0.0306 Hz to about 0.0187 Hz. Moreover, the recovery time is also significantly shorter. In addition, under the emergency traction scenario, the original maximum frequency deviation deteriorates to about 0.0235 Hz. However, by using the proposed method, the maximum frequency deviation can be reduced to only about 0.0144 Hz, which is only 61.28% of the original value. And the recovery time is also markedly reduced from about 10.11 s to about 4.63 s, which is only 45.80% of the original value.

Results of these cases imply that the proposed REFR method is high-performance, i.e., small frequency deviation and fast frequency recovery, even with abrupt steeps in electric load. Therefore, our proposed method can contribute to the frequency stability of power systems during these emergency events.

4.5. Frequency regulation performance with communication time delay

In this part, it is assumed that there are communication time delays in the control process of the power system frequency regulation. There are four scenarios employed to verify the effectiveness of the proposed method with communication time delays of 50 ms, 100 ms, 200 ms, and 300 ms, respectively. The results of these communication time delays are illustrated in Fig. 9.

It is shown in Fig. 9, without the proposed method, the maximum frequency deviation is deteriorated due to the communication time delays. However, by using the proposed method, this index can be improved significantly. Moreover, without the proposed method, different levels of system frequency oscillation occur, which may cause severe damage to the power system. However, by using the proposed

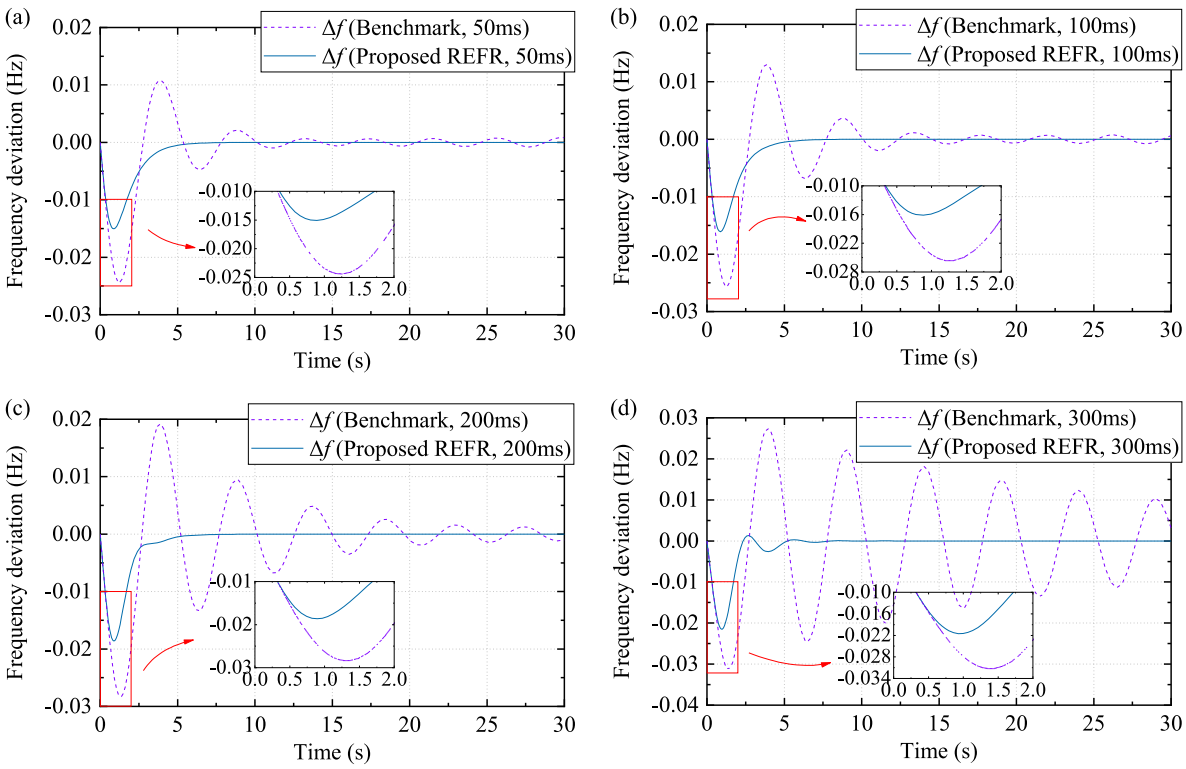

Fig. 9. Frequency regulation performance with communication time delay (a) 50 ms; (b) 100 ms; (c) 200 ms; (d) 300 ms.

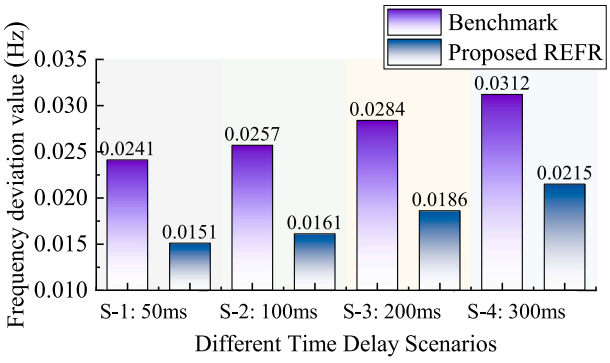

Fig. 10. The maximum frequency deviation caparison under different communication delay scenarios.

method, the system frequency can always converge to the scheduled frequency rapidly, and there is no system frequency oscillation, even with different levels of communication time delay.

Specifically, take the fourth scenario as an example. From Fig. 9(d), due to the communication time delay, the maximum frequency deviation would have deteriorated to about 0.0312 Hz. However, this index can be improved to about 0.0215 Hz by using the proposed method. In addition, as shown in Fig. 9(d), because of the communication time delay, the system frequency oscillation would have occurred, and the system frequency would no longer converge to the scheduled frequency. This is reasonable since the control decision is according to the detected frequency information, and the information with a time delay can mislead the control center, thus leading to an opposite regulation and even causing the frequency oscillation. However, by using the proposed method, the system frequency can still converge to the scheduled frequency, and the recovery time achieves only about 4.96 s. This implies the system frequency can rapidly converge to the scheduled frequency with our proposed method, even under the communication time delay condition.

In addition, the maximum frequency deviation in these different scenarios with communication time delay is compared and illustrated in Fig. 10.

As shown in Fig. 10, by using the proposed REFR method, the maximum frequency deviation is improved from 0.0241 Hz to 0.0151 Hz, from 0.0257 Hz to 0.0161 Hz, from 0.0284 Hz to 0.0186 Hz, and from 0.0312 Hz to 0.0215 Hz in four scenarios with communication time delay, respectively. This implies that even with the communication time delay, the maximum frequency deviation can be significantly improved by the proposed REFR method. Therefore, our method is helpful for the power system to overcome the negative impact caused by communication time delays.

4.6. Frequency regulation performance with multiple cyber–physical emergency events

To verify the effectiveness of the proposed method in a complicated situation with multiple emergencies in the both cyber layer and physical layer, this case takes into account accidental generator outage, abrupt steep in electric load, and communication time delay comprehensively and simultaneously.

The test process is as follows: at 20 s, an emergency braking event occurs in the power system; at 50 s, an accidental generator outage occurs; then, at 100 s, a communication time delay occurs, which is an emergency event in cyber layer, and it lasts until 200 s; at the same time, at 100 s, another emergency braking event occurs; then, at 170 s, another accidental generator outage occurs; at 200 s, the communication time delay ends, and communication is returned to normal; then, at 250 s, an emergency traction event occurs; and finally, this test ends at 300 s, for a total test time of 300 s. The results of these multiple cyber and physical emergency events are illustrated in Fig. 11.

According to Fig. 11, it is shown that the system frequency deviates affected by the multiple emergency events. Especially when there is

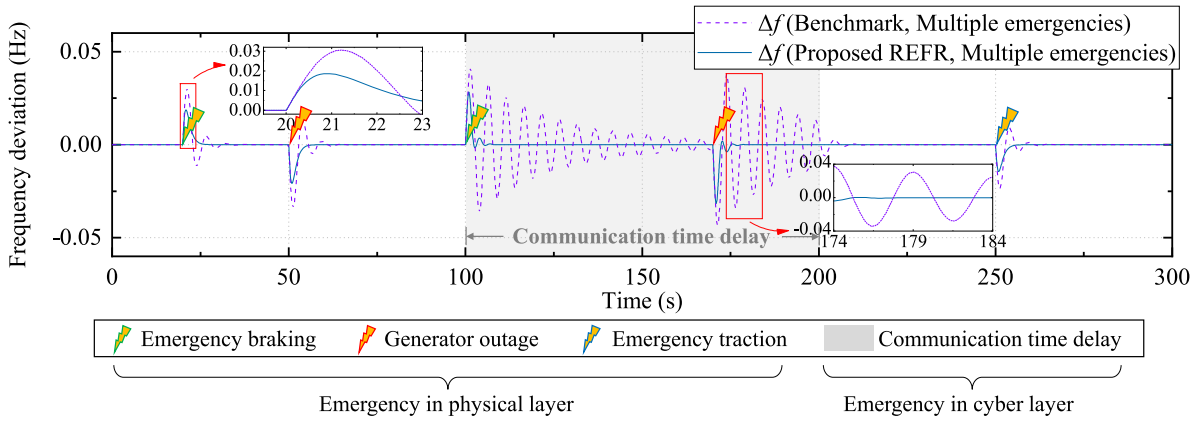

Fig. 11. Frequency regulation performance with multiple cyber and physical emergency events.

a communication time delay, emergency events in cyber layer and physical occur simultaneously at this time band (from 100 to 200 s). As a result, the frequency oscillation occurs, and the system frequency cannot converge to scheduled frequency anymore. This means the frequency of the power system has deteriorated severely. However, by using our proposed REFR method, the system frequency can always be promptly regulated to the scheduled frequency, even in such complicated situations with multiple emergencies.

To show more specifics, the two spikes in Fig. 11 are enlarged to show details of the curves. In the first enlarged view, the maximum frequency deviation without and with the proposed REFR method is 0.0306 Hz and 0.0187 Hz, respectively. And the recovery time without and with the proposed REFR method is 10.28 s and 4.77 s, respectively. That is to say, by using the proposed method, the maximum frequency deviation and the recovery time can be improved to about 61.11% and 46.40% of the original value, respectively. In the second enlarged view, the system frequency is affected by multiple cyber and physical emergency events simultaneously. The maximum frequency deviation is 0.0432 Hz and 0.0316 Hz without and with the proposed method, respectively. And without the proposed method, frequency oscillation occurs, and the system frequency is hard to converge back to the scheduled frequency. However, benefiting from the proposed method, the system frequency can be regulated to the scheduled frequency after only about 4.98 s of the multiple emergency events. These results show the REFR method can still be effective in improving frequency performance even with multiple emergencies simultaneously.

4.7. Frequency regulation performance with emergency events over a long period of time

In order to validate the effectiveness of the proposed REFR method over a long time, the test is carried out for 24 h (0:00–24:00) considering emergency events, including accidental generator outages, abrupt steeps in electric load, and communication time delay. Each emergency event has two states, 0-state and 1-state. The 0-state indicates the normal state, i.e., the emergency event does not occur, while the 1-state indicates the emergency state, i.e., the emergency event occurs. The time duration of each emergency event's state is assumed to follow a Gaussian distribution, as detailed in Table 1.

As described in Table 1, the time duration of the accidental generator outage event in emergency state obeys a Gaussian distribution with a mean value of 1 h and a standard deviation of 15 min. And in normal state, the time duration of this event obeys a Gaussian distribution with a mean of 4 h and a standard deviation of 1 h. Besides, the time duration of the communication time delay event in emergency state and normal state obeys a Gaussian distribution with a mean value of 3 min and a standard deviation of 1 min and a Gaussian distribution with a mean of 6 h and a standard deviation of 1.5 h, respectively. This implies

Table 1
Parameters of Gaussian distribution for the time duration of emergency events.

Emergency event	State[a]	Mean		Standard deviation	
		Value	Unit	Value	Unit
Accidental generator outage	1-state	1	hour	0.25	hour
	0-state	4	hour	1	hour
Abrupt steep in electric load	1-state	60	sec	20	sec
	0-state	3	hour	1	hour
Communication time delay	1-state	180	sec	60	sec
	0-state	6	hour	1.5	hour

[a]The 0-state denotes the normal state, and the 1-state denotes the emergency state.

that these cyber and physical emergencies can occur during the whole testing process. Therefore, the proposed method has to counter against all of these emergency events occurring within a 24-hour period. The results of this long period of time test are illustrated in Fig. 12.

From Fig. 12(a), it can be observed that within the 24-hour period, dozens of cyber–physical emergency events occurred, resulting in system frequency deviations. It is practical, since actually emergencies in the power system do not just appear once and then never happen again, but can occur many times over a period of time. However, with the proposed REFR method, these emergencies can always be accommodated, and the system frequency can be regulated to the scheduled frequency rapidly over this long period of time. This implies the proposed method can continuously regulate the power system frequency to counter against a lot of emergency events.

In addition, from the detailed performance graphs from Fig. 12(b), (c), and (d), it is found that due to emergency events, the system frequency deteriorates severely, and even frequency oscillations occur. However, with the proposed method, the maximum frequency deviation becomes noticeably more minor, the recovery time of system frequency is remarkably shortened, and even the original frequency oscillations can be avoided. This means that by using the proposed method, the frequency performance of the power system is significantly improved.

Therefore, the proposed method can continuously contribute to the power system frequency regulation with multiple cyber and physical emergency events over a long period of time.

5. Conclusion

In order to counter against multiple cyber and physical emergency events and guarantee power energy security, a REFR scheme is proposed for the power system to achieve high-performance frequency regulation. First, a virtual auxiliary surface is constructed based on the coordinate transformation technique to ensure the system frequency stability. On this basis, a robust controller is developed to achieve a

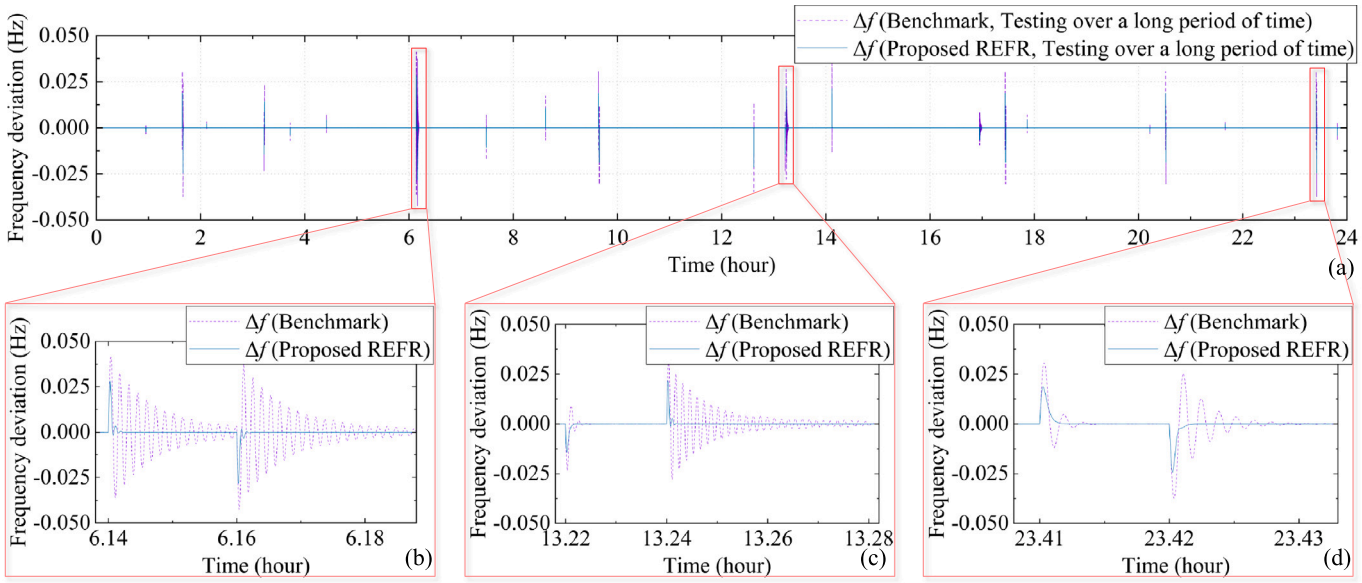

Fig. 12. Frequency regulation performance with emergency events: (a) Performance over a long period of time; (b), (c), and (d) Detailed performance graphs.

minor frequency deviation and a faster recovery for frequency regulation. In addition, rigorous proofs show that stability can be guaranteed by the proposed method, despite multiple emergency events.

The results of case studies show that the recovery speed of system frequency becomes faster by benefiting from the proposed method, up to 46.40% of the original one. Moreover, the maximum frequency deviation can also be improved to about 61.11% of the original value by using the proposed REFR method, which implies that the frequency fluctuation during the regulation process can be mitigated remarkably. In addition, in a complicated situation with multiple emergency events in cyber and physical layer simultaneously, the frequency oscillation occurs, and the system frequency cannot converge to the scheduled frequency anymore. However, by using our proposed method, the frequency deviation can still converge to zero within about 4.98s, even with multiple emergencies. Therefore, the effectiveness of the proposed REFR scheme is verified, and it can withstand multiple cyber and physical emergency events, thus contributing to the frequency regulation of the power system.

CRediT authorship contribution statement

Shaohua Yang: Writing – review & editing, Writing – original draft, Visualization, Validation, Software, Methodology, Investigation, Formal analysis, Conceptualization. **Keng-Weng Lao:** Writing – review & editing, Supervision, Resources, Project administration, Funding acquisition. **Hongxun Hui:** Writing – review & editing, Supervision, Resources, Data curation. **Yulin Chen:** Writing – review & editing, Supervision, Resources, Data curation.

Declaration of competing interest

The authors declare that they have no known competing financial interests or personal relationships that could have appeared to influence the work reported in this paper.

Data availability

The authors do not have permission to share data.

Acknowledgments

This work was partly funded by The Science and Technology Development Fund, Macau SAR (Grant/Project no. SKL-IOTSC(UM)-2021-2023, 0003/2020/AKP, and FDCT/0022/2020/A1).

References

[1] Yan J. Energy systems in transition: Challenges and opportunities. Adv Appl Energy 2020;1:100005.
[2] Xie D, Xu Y, Nadarajan S, Viswanathan V, Gupta AK. Dynamic frequency-constrained load restoration considering multi-phase cold load pickup behaviors. IEEE Trans Power Syst 2023. http://dx.doi.org/10.1109/TPWRS.2022.3225798, Early Access.
[3] MacIver C, Bell K, Nedd M. An analysis of the August 9th 2019 GB transmission system frequency incident. Electr Power Syst Res 2021;199:107444.
[4] Hui H, Ding Y, Song Y. Adaptive time-delay control of flexible loads in power systems facing accidental outages. Appl Energy 2020;275:115321.
[5] Ma Y, Hu Z, Song Y. Hour-ahead optimization strategy for shared energy storage of renewable energy power stations to provide frequency regulation service. IEEE Trans Sustain Energy 2022;13(4):2331–42.
[6] Sang M, Ding Y, Bao M, Song Y, Wang P. Enhancing resilience of integrated electricity-gas systems: A skeleton-network based strategy. Adv Appl Energy 2022;7:100101.
[7] Liu X, Li Y, Lin X, Guo J, Shi Y, Shen Y. Dynamic bidding strategy for a demand response aggregator in the frequency regulation market. Appl Energy 2022;314:118998.
[8] Rodrigues YR, Abdelaziz M, Wang L. D-PMU based secondary frequency control for islanded microgrids. IEEE Trans Smart Grid 2019;11(1):857–72.
[9] Mejia-Ruiz GE, Paternina MRA, Segundo Sevilla FR, Korba P. Fast hierarchical coordinated controller for distributed battery energy storage systems to mitigate voltage and frequency deviations. Appl Energy 2022;323:119622.
[10] Shuai B, Zhou Q, Li J, He Y, Li Z, Williams H, et al. Heuristic action execution for energy efficient charge-sustaining control of connected hybrid vehicles with model-free double Q-learning. Appl Energy 2020;267:114900.
[11] Chen Y, Lao K-W, Qi D, Hui H, Yang S, Yan Y, et al. Distributed self-triggered control for frequency restoration and active power sharing in islanded microgrids. IEEE Trans Ind Inf 2023;19(10):10635–46.
[12] Liu H, Pan H, Wang N, Yousaf MZ, Goh HH, Rahman S. Robust under-frequency load shedding with electric vehicles under wind power and commute uncertainties. IEEE Trans Smart Grid 2022;13(5):3676–87.
[13] Baruwa M, Fazeli M. Impact of virtual synchronous machines on low-frequency oscillations in power systems. IEEE Trans Power Syst 2021;36(3):1934–46.
[14] Estevez PG, Marchi P, Messina F, Galarza C. Forced oscillation identification and filtering from multi-channel time-frequency representation. IEEE Trans Power Syst 2023;38(2):1257–69.
[15] Chen Y, Qi D, Hui H, Yang S, Gu Y, Yan Y, et al. Self-triggered coordination of distributed renewable generators for frequency restoration in islanded microgrids: A low communication and computation strategy. Adv Appl Energy 2023;10:100128.
[16] Cai S, Matsuhashi R. Optimal dispatching control of EV aggregators for load frequency control with high efficiency of EV utilization. Appl Energy 2022;319:119233.
[17] Hui H, Chen Y, Yang S, Zhang H, Jiang T. Coordination control of distributed generators and load resources for frequency restoration in isolated urban microgrids. Appl Energy 2022;327:120116.

[18] Xie K, Hui H, Ding Y, Song Y, Ye C, Zheng W, et al. Modeling and control of central air conditionings for providing regulation services for power systems. Appl Energy 2022;315:119035.
[19] Bünning F, Heer P, Smith RS, Lygeros J. Increasing electrical reserve provision in districts by exploiting energy flexibility of buildings with robust model predictive control. Adv Appl Energy 2023;10:100130.
[20] Li H, Ren Z, Fan M, Li W, Xu Y, Jiang Y, et al. A review of scenario analysis methods in planning and operation of modern power systems: Methodologies, applications, and challenges. Electr Power Syst Res 2022;205:107722.
[21] Singh V, Moger T, Jena D. Probabilistic load flow for wind integrated power system considering node power uncertainties and random branch outages. IEEE Trans Sustain Energy 2023;14(1):482–9.
[22] Zheng W, Li J, Lei K, Shao Z, Li J, Xu Z. Optimal dispatch of HCNG penetrated integrated energy system based on modelling of HCNG process. Int J Hydrogen Energy 2023;48(51):19437–49.
[23] Hui H, Siano P, Ding Y, Yu P, Song Y, Zhang H, et al. A transactive energy framework for inverter-based HVAC loads in a real-time local electricity market considering distributed energy resources. IEEE Trans Ind Inf 2022;18(12):8409–21.
[24] Qiu D, Dong Z, Ruan G, Zhong H, Strbac G, Kang C. Strategic retail pricing and demand bidding of retailers in electricity market: A data-driven chance-constrained programming. Adv Appl Energy 2022;7:100100.
[25] Zheng W, Li J, Shao Z, Lei K, Li J, Xu Z. Optimal dispatch of hydrogen/electric vehicle charging station based on charging decision prediction. Int J Hydrogen Energy 2023. http://dx.doi.org/10.1016/j.ijhydene.2023.03.375, Early Access.
[26] Yang S, Lao K-W, Hui H, Chen Y, Dai N. Real-time harmonic contribution evaluation considering multiple dynamic customers. CSEE J Power Energy Syst 2023. http://dx.doi.org/10.17775/CSEEJPES.2022.06570, Early Access.
[27] Wang S, Hui H, Ding Y, Ye C, Zheng M. Operational reliability evaluation of urban multi-energy systems with equivalent energy storage. IEEE Trans Ind Appl 2023;59(2):2186–201.
[28] Products & Service. CRRC YONGJI ELECTRIC CO., LTD. Official Website. Tech. rep., 2023, [Online]. Available: https://www.crrcgc.cc/yjdjen.
[29] Liu L, Zhou Z, Dai N, Lao K-W, Song Y. Interpolated phase-shifted PWM for harmonics suppression of multilevel hybrid railway power conditioner in traction power supply system. IEEE Trans Transp Electr 2022;8(1):898–908.
[30] Hosseini SA, Toulabi M, Dobakhshari AS, Ashouri-Zadeh A, Ranjbar AM. Delay compensation of demand response and adaptive disturbance rejection applied to power system frequency control. IEEE Trans Power Syst 2020;35(3):2037–46.
[31] Qiu Y, Lin J, Liu F, Dai N, Song Y. Continuous random process modeling of AGC signals based on stochastic differential equations. IEEE Trans Power Syst 2021;36(5):4575–87.
[32] Hui H, Ding Y, Song Y, Rahman S. Modeling and control of flexible loads for frequency regulation services considering compensation of communication latency and detection error. Appl Energy 2019;250:161–74.
[33] Su J, Zhang H, Liu H, Yu L, Tan Z. Membership-function-based secondary frequency regulation for distributed energy resources in islanded microgrids with communication delay compensation. IEEE Trans Sustain Energy 2023. http://dx.doi.org/10.1109/TSTE.2023.3266295, Early Access.
[34] Wang S, Zhai J, Hui H. Optimal energy flow in integrated electricity and gas systems with injection of alternative gas. IEEE Trans Sustain Energy 2023;14(3):1540–57.
[35] Shi Q, Li F, Cui H. Analytical method to aggregate multi-machine SFR model with applications in power system dynamic studies. IEEE Trans Power Syst 2018;33(6):6355–67.
[36] Liu J, Gu Y, Zha L, Liu Y, Cao J. Event-triggered H_∞ load frequency control for multiarea power systems under hybrid cyber attacks. IEEE Trans Syst Man Cybern 2019;49(8):1665–78.
[37] Wang P, Zhang Z, Ma T, Huang Q, Lee W-J. Parameter calibration of wind farm with error tracing technique and correlated parameter identification. IEEE Trans Power Syst 2022. http://dx.doi.org/10.1109/TPWRS.2022.3232627, Early Access.
[38] Yang S, Lao K-W, Chen Y, Hui H. Resilient distributed control against false data injection attacks for demand response. IEEE Trans Power Syst 2023. http://dx.doi.org/10.1109/TPWRS.2023.3287205, Early Access.